

Article

Sintering Behaviors of Carbon Nanotubes—Aluminum Composite Powders

Biao Chen * and Katsuyoshi Kondoh

Joining and Welding Research Institute, Osaka University, 11-1 Mihogaoka, Ibaraki, Osaka 567-0047, Japan; kondoh@jwri.osaka-u.ac.jp

* Correspondence: chen-b@jwri.osaka-u.ac.jp; Tel.: +81-6-6879-8669

Academic Editor: Hugo F. Lopez

Received: 8 July 2016; Accepted: 31 August 2016; Published: 6 September 2016

Abstract: Carbon nanotubes (CNTs) are promising reinforcements for fabricating aluminum (Al) matrix composites with outstanding properties. The understanding of the consolidation process of CNT-Al composite powders plays a significant role in achieving high performances of bulk composites. In this study, an advanced consolidation technique of spark plasma sintering (SPS) was used to fabricate CNT-Al composites with homogeneously dispersed CNTs. The sintering kinetics of pure Al powders and those powders coated with 1 wt % CNTs were studied. By combining the electrical conductivity and relative density results, it was found that the sintering process consisted of two stages with distinct densification rates. The second stage with a much lower rate was governed by the breaking down of alumina films at primary particle boundaries. The activation energy of the controlling second stage increased by 55% in CNT-Al composite powders compared to that of pure Al powder. As a result, CNT addition led to the overall decrease of sintering ability, which raised a challenge in the processing of CNT-Al composites.

Keywords: carbon nanotubes; metal matrix composites; spark plasma sintering; density; electrical conductivity; sintering kinetics

1. Introduction

Carbon nanotubes (CNTs), including multi-walled CNTs and single-walled CNTs, have attracted great attention in materials science since the landmark report by Iijima in 1991 [1]. Due to the outstanding structural and physical properties, such as large aspect ratios, high strength, and high electrical/thermal conductivities, CNTs are regarded as promising reinforcements for composites [2]. In the past decade, increasing attention was paid to CNT reinforced metal matrix composites (MMCs), which were expected as next-generation strong materials [3]. Special interests were paid to aluminum (Al) matrix composites (AMCs) because their high specific strength, high conductivities, and anti-corrosive properties made them promising structural materials in aerospace, automobile, and sports industries [4].

To achieve high load transfer efficiency [5] in CNT-Al composites, suitable processing approaches should be explored. A homogeneous CNT dispersion in composites is the precondition, because there is little bonding between matrix and the CNTs inside CNT clusters, which is detrimental for effective load transfer [6]. To overcome the problems of CNT agglomeration, some novel methods, such as the in-situ grown method [7], flake powder metallurgy [8], friction stir welding [9], and solution ball milling (SBM) [10], have been recently developed. Afterward, how to effectively consolidate CNT-Al powder mixtures to bulk materials became a concentrated topic. To make most use of CNTs, optimal composite structures are demanded for the consolidation process. Among the diverse microstructures, a high relative density is the first consideration, because it is the prime requirement for effective CNT-Al bonding in CNT-Al composites fabricated by powder metallurgy. There are a number of

candidates for consolidating, for example, casting [11], rolling [12], extrusion [13], sintering [14], and a combination of sintering and extrusion [15]. Among them, sintering is a promising one, mainly because of the comparatively low processing temperature, flexibility, and low cost.

Spark plasma sintering (SPS) is an advanced sintering technique where a pulsed direct current is applied to pass through the powder compact. Compared with conventional sintering techniques, SPS can produce higher sample densities (near full density) under low-temperature conditions [16]. It is a significant advantage in those powder systems where grain growth or severe reactions had to be avoided. For example, a severe interfacial reaction between CNTs and Al, happening at a high processing temperature near the melting point of Al, would ruin the structure of CNTs [17]. Therefore, SPS has been popular for the consolidation of many advanced nanocomposite powder systems [18]. A number of studies have also used the combination of SPS and extrusion to fabricate CNT-Al composites [3,5,6,10,16,19]. However, the applicability of SPS for fabricating high-performance composites is still unclear. To examine this issue, the understanding on the sintering behaviors of CNT-Al composites powders is required primarily.

In this study, SPS was applied to consolidate the CNT-Al composite powders containing 1 wt % well-dispersed CNTs. As other processing conditions were fixed, SPS temperature was varied at 700, 750, 800, 850, and 900 K (melting point of pure Al, T_m , is ~933 K). The microstructural and conductive properties of as-sintered CNT-Al composites were systematically characterized. It was found that a critical temperature (T_c) corresponded to the transformation of the sintering regime existed during the consolidation of pure Al and CNT-Al composite powders. The CNT addition led to the decreased sintering rate and ~50 K delay of T_c . However, at high SPS temperature of 900 K, CNT-Al composite had a high relative density and high electrical conductivity, which were similar to those of pure Al. The effect of the observed alumina impurity on sintering kinetic of CNT-Al composite powder was discussed.

2. Materials and Methods

In this study, a mechanical coating process was used to obtain homogeneous CNT dispersion in AMCs. Pure Al powders (99.9% purity, Kojundo Chemical Laboratory Co., Saitama, Japan) was first milled with 2 wt % stearic acid (process control agent) powders using a planetary ball milling machine. The powders were sealed in a ZrO_2 jar together with ZrO_2 milling balls in an argon gas atmosphere. The revolution speed was 200 rpm, and milling time was 240 min. The milled powder was heat-treated at 700 K for 30 min in a vacuum furnace to remove the stearic acid. The next step is to disperse CNTs on prepared flaky Al powder surface. Multi-walled CNT (Baytubes C150P, Bayer Material Science Co., Tokyo, Japan) was used in this study. Flaky Al powders bathed in isopropyl alcohol (IPA)-based solution with ~1 wt % zwitterionic surfactants and 1 wt % CNTs in a plastic bottle on a rocking ball milling machine for 120 min. ZrO_2 milling balls were added to assist the coating of CNTs on flaky powders. The powder mixture was heat-treated at 700 K for 30 min in a vacuum furnace to remove the remained surfactants.

The obtained CNT-Al composite powders were then consolidated by SPS on a SPS system (SPS-1030S, SPS Syntex, Kawasaki, Japan) at various sintering temperatures of 700 K ($0.75T_m$), 750 K, 800 K, 850 K, and 900 K ($0.96T_m$) with a heating rate of $20 \text{ K} \cdot \text{min}^{-1}$, and held at each temperature for 60 min at pressure of 30 MPa under vacuum of 5 Pa. Graphite container (42 mm in inner-diameter) and graphite punches (42 mm in diameter) were used to hold the powders. Before sintering, the powder compacts were pressed under 10 MPa for 5 s. After the holding stage, the SPS power was switched off, and the sintered samples were cooled down inside the chamber. The samples were taken out below 373 K. More details on the process can be found elsewhere [20].

The morphology of Al powder, CNT powder, Al-CNT composite powder, and as-sintered CNT-Al composites were examined by field emission scanning electron microscopy (FE-SEM, JEM-6500F, JEOL, Tokyo, Japan). Before SEM observation, the as-sintered samples were mechanically polished and then deeply chemically etched using an acid solution with 25% HNO_3 , 15% HCl, 10% HF, and 50% H_2O in

volume. The microstructure of CNT-Al composites were also characterized by transmission electron microscopy (TEM, JEM-2010, JEOL, Tokyo, Japan), assisted with energy Dispersive Spectrum (EDS). The density of sintered samples were measured on an ELECTRONIC DENSIMETER device (MDS-300, ALFA MIRAGE CO., LTD., Osaka, Japan) based on the Archimedes' method. Three density values were used to get an average value. The relative density was further estimated using density of Al and CNT as 2.7 and 2.0 g·cm⁻³, respectively. The electrical conductivity was measured by a portable eddy current tester (AutoSigma3000, Tokyo, Japan) with a testing probe size of 8 mm in diameter. Thirty values were obtained at different positions to get an average conductivity.

3. Results

Figure 1 shows the morphologies of the starting Al and CNT powders. Starting Al powders have a near-spherical shape with an average diameter of ~20 µm (Figure 1a). The starting CNTs are agglomerated under the strong Van der Waals force (Figure 1b). CNTs have a slender shape with a large aspect ratio (~15 nm in diameter and ~1 µm in length). Large aspect ratios are favorable to achieve high load transfer efficiency of CNTs in composites [5].

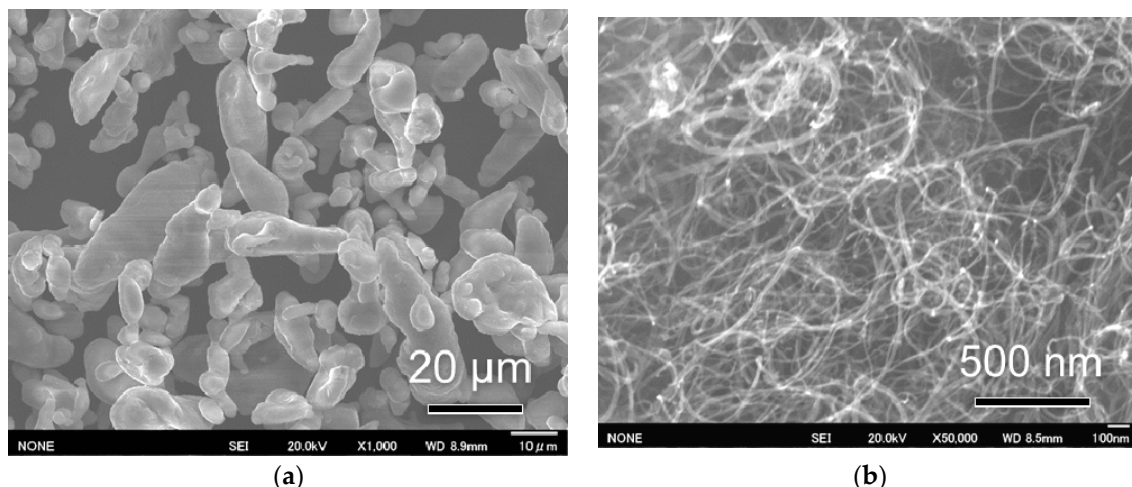


Figure 1. Morphology of starting materials: (a) pure Al powder; (b) CNT powder.

Figure 2 shows the morphology of fabricated flaky Al powder surface coated with 1 wt % CNTs. After ball milling for 240 min, Al powders changed from near-spherical (Figure 1a) to flaky morphology with a thickness of several microns (Figure 2a). Some small flakes were cold-welded to a large one with a thickness of several tens of microns. Formation of flaky powders were attributed to the good plastic deformability and the assistant effect of stearic acid. The flattening and welding of Al powders were common phenomena observed in the high-energy ball milling process [8,13]. A very uniform CNT dispersion was observed at a high-magnification view on the powder surface (Figure 2b). The CNTs were homogeneously and randomly distributed on the flattened surface. The overlaps between CNTs were limited, suggesting a high dispersion quality. Compared with the previous solution coating process [21], improved CNT dispersion was achieved in the present process due to the dynamic blending-assisted dispersion of CNTs [10].

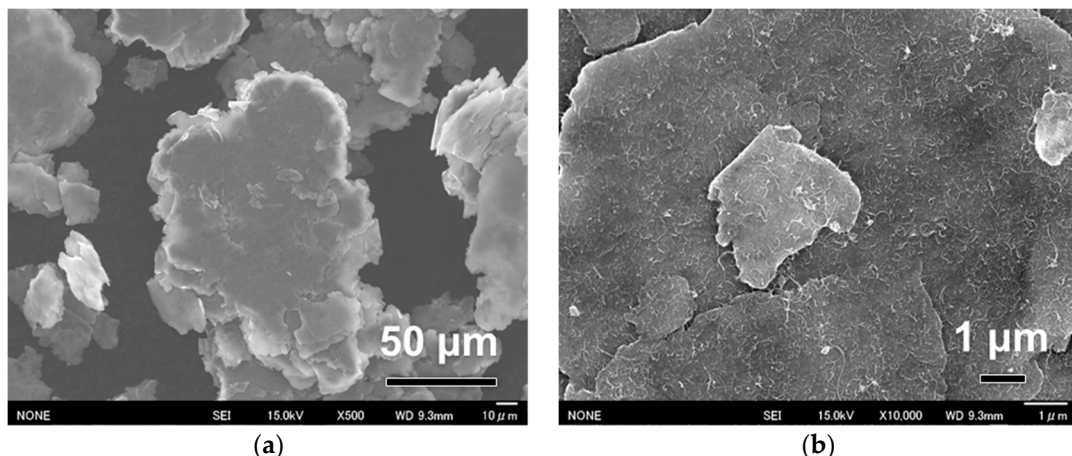


Figure 2. Morphology of CNT–Al composite powder dispersed by mechanical coating process at different magnifications: (a) Flattened surfaces were produced of flaky Al powders; (b) CNTs were uniformly distributed on the flaky powder surface.

Figure 3 shows the measured electrical conductivity of the as-sintered pure Al and CNT–Al composites. It can be seen that the conductivity-temperature curves of both pure Al and CNT–Al composites exhibited two stages, divided by a critical temperature (T_c) where the tendency transformed. At Stage I below T_c , the conductivities were quite low, nearly zero. At Stage II beyond T_c , the electrical conductivities dramatically improved with increasing temperature. T_c was 750 K for pure Al, and it was 800 K for CNT–Al composites, suggesting a ~50 K increase of T_c by adding CNTs in the Al matrix.

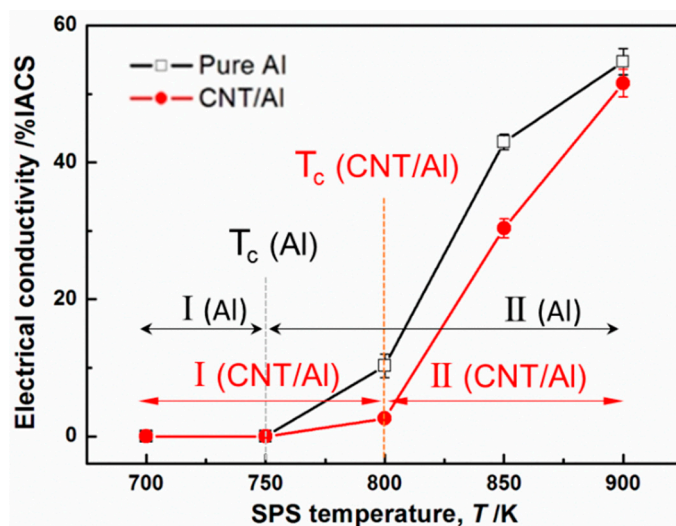


Figure 3. Electrical conductivity of pure Al and CNT–Al composites sintered under different temperatures.

The densification analyses of pure Al and CNT–Al composite powders are shown in Figure 4. With increasing SPS temperature, the relative density (ρ) of pure Al and CNT–Al composites increased continuously. Under each temperature, ρ of CNT–Al composites was smaller than that of pure Al. However, the difference became smaller at high temperatures. Even at 900 K, pure Al and CNT–Al composite showed similar values of ~99%. To clarify the kinetics of densification, the Arrhenius law was applied to estimate the activation energy (E_a) of sintering [22]:

$$\ln \rho = \ln \rho_0 - \frac{E_a}{RT} \quad (1)$$

where ρ_0 is a constant value. E_a can be estimated from the slope of the curve of $\ln \rho - (1/T)$. Figure 4b shows the plotted curves. It was interesting to find the two materials also had two stages whose E_a values were distinct. The two stages were coincident with those found in the conductivity-temperature curves (Figure 3). After T_c , Stage II had increased E_a compared with that of Stage I. Moreover, it was observed that CNT-Al composites had larger activation energy values than pure Al at the two stages. For example, at Stage II, E_a was $5.53 \text{ kJ} \cdot \text{mol}^{-1}$ for CNT-Al and $3.57 \text{ kJ} \cdot \text{mol}^{-1}$ for pure Al, showing a 55% increment from pure Al to the CNT-Al composite. This suggests that the sintering rate of pure Al powder significantly decreased when CNTs were added.

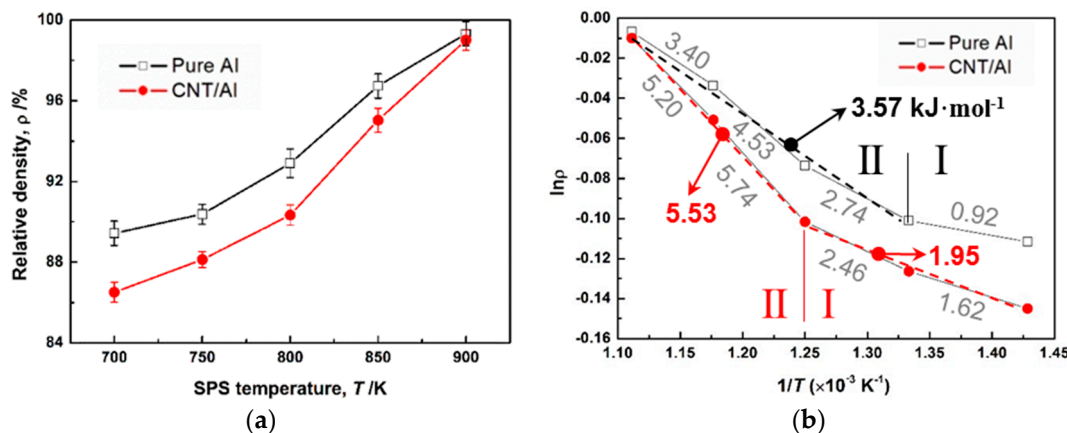


Figure 4. Sintering kinetics of pure Al and CNT-Al composites: (a) Relation between relative density (ρ) and SPS temperature (T). (b) Relation between $\ln \rho$ and $1/T$. The activation energy of sintering estimated from the slop is shown in (b).

The polishing microstructure of CNT-Al composite sintered at 900 K is shown in Figure 5. After chemical etching, the primary particle boundaries were revealed to show the boundaries between flaky Al powders, as observed in the white flow lines in Figure 5a. From the high-magnification view on a primary particle boundary (Figure 5b), a remained oxide film was observed which departed from the two powder particles.

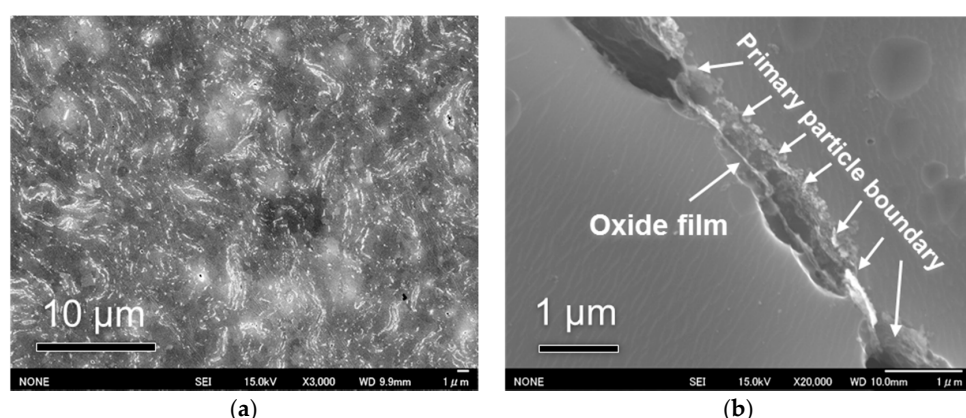


Figure 5. Microstructure of CNT-Al composite sintered at 900 K at different magnifications. (a) A low-magnification view. (b) A local view.

To confirm the oxide films, EDS-assisted TEM analysis was performed on CNT-Al sintered at 900 K, as shown in Figure 6. Many discontinuous secondary phases were observed in the Al matrix (Figure 6a). The phases had fibrous and disk-like shapes. From the EDS maps (Figure 6b,c), these phases were less rich in Al and high concentrations of oxygen. Considering the low solubility of

oxygen in Al, these phases can be identified as aluminum oxide or alumina, which has been commonly observed in powder metallurgy Al materials. Some carbon-concentrated areas were also observed from the carbon element distribution (as arrows indicated in Figure 6d). It was corresponded to the CNT distribution in the Al matrix.

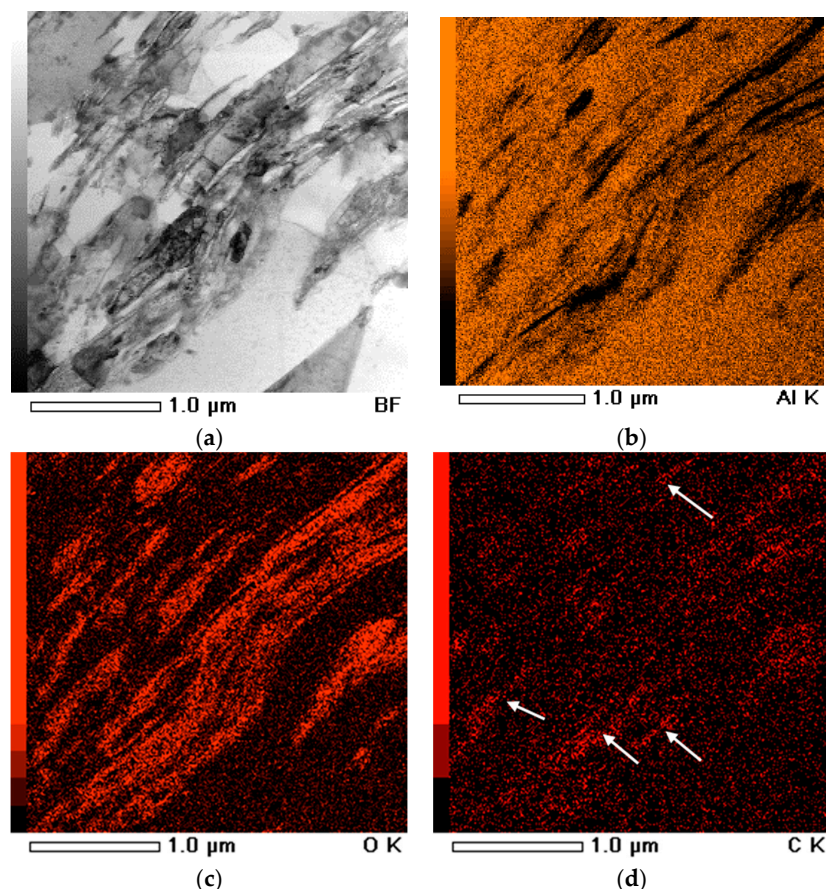


Figure 6. Combination of TEM and EDS analyses on composite CNT–Al sintered at 900 K. (a) Bright field TEM image. (b) Al element distribution. (c) Oxygen (O) element distribution. (d) Carbon (C) element distribution.

4. Discussion

This study revealed that there were two sintering stages for pure Al powders that experienced the ball milling process and those powders coated with CNTs. The two stages had distinct sintering rates. Stage I had higher rates than those in Stage II in the two materials (Figure 4b). In Stage I, the electrical conductivity was very low near 0, suggesting the high electron transfer resistance [6] through primary particle boundaries, which were mainly made of alumina films (Figure 5). It has been reported that, as ball milling was applied to Al powders, a high oxygen concentration was produced, resulting in more and thicker alumina films [8]. Therefore, at Stage I, the diffusion of oxygen atoms and the morphology change of the alumina film might be small. The increase of relative density is mainly attributed to the deformation of Al powders. This stage had a small activation energy of $0.92 \text{ kJ}\cdot\text{mol}^{-1}$ for pure Al and $1.95 \text{ kJ}\cdot\text{mol}^{-1}$ for the CNT–Al composite. This suggests a high densification rate at this stage, which is possibly a result of the disappearance of large pores between powders. At Stage II, the electrical conductivities increased rapidly as sintering temperature increased (Figure 2). This suggests that the alumina film at primary particle boundaries started to be physically or chemically broken down. Adjacent Al grains can be bonded together for the effective electron transfer. Due to the existence of alumina films, the densification rates noticeably decreased with those

of Stage I, as seen from the great difference in activation energy values (Figure 4b). Therefore, Stage II, where the alumina films were broken down, was the controlling process for the sintering of Al and CNT-Al powders. The alumina film played a dominant role in deciding the sintering kinetic of Al powders.

With CNT additions, the sintering rate at Stages I and II decreased compared with pure Al without CNTs. This indicates that CNTs were disadvantageous to the deformation of Al powders and the breaking of alumina film at powder boundaries. The decreased deformability of CNT-Al composite powders at elevated temperatures can reasonably be attributed to the improved hardness and modulus by adding CNTs [3]. The decreased breaking ability of alumina film is possibly due to the fact that the CNTs between alumina films (Figure 6d) acted as shields that blocked the diffusion of oxygen atoms and consequently suppressed the breaking down of alumina films. As a result, the sintering rate of CNT-Al composite powder greatly decreased, which indicates that it would be a challenge for future studies to fabricate full-density composites exhibiting excellent properties.

Severe plastic deformation (SPD) processes after SPS, such as rolling and extrusion, may be good candidates to overcome this raised challenge. The combination of SPS and SPD processes could give nearly full density to CNT-Al composites [17,19]. However, the problem of poor bonding condition in as-sintered samples still remains in the SPD materials [20]. It suggests that the sintering behaviors during SPS still showed great effect on the bonding conditions and properties of final SPD composites under the same sintering time. A high SPS temperature seemed essential to effectively breaking down the alumina film for achieving effective bonding at Al-Al boundaries and CNT-Al interfaces. This thus well explained the overall property improvement of the CNT-Al composite sintered at 900 K, such as conductivity (Figure 3), while severe interfacial reaction was a potential problem at high SPS temperatures. A balance of relative density and interfacial reaction at a suitable SPS temperature should be explored in future studies to achieve overall excellent performances.

5. Conclusions

The sintering behaviors of ball milled pure Al powders and those powders coated with well-dispersed CNTs were studied using the Arrhenius law. The sintering process consisted of two stages with distinct densification kinetics, agreeing with the tendencies of electrical conductivities. The second stage with a lower densification rate, which was governed by the breaking down of alumina films at primary particle boundaries, was a controlling process in SPS. CNT additions led to the overall decrease of sintering kinetics. The activation energy of the controlling Stage II increased by 55% in CNT-Al composite powder compared with that of pure Al powder, which raised the challenge of fabricating full-density composites. At a high SPS temperature of 900 K, the density and electrical conductivity of composites reached the similar level of pure Al. Taking the balance of relative density and interfacial conditions into account, suitable SPS conditions should be explored to achieve the optimal mechanical and conductive properties.

Acknowledgments: The authors would like to thank the support of TEM observations by Makoto Takahashi from JWRI, Osaka University, Japan.

Author Contributions: B.C. performed the experiments, analyzed the data, and wrote the paper. K.K. supervised the project.

Conflicts of Interest: The authors declare no conflict of interest.

References

1. Iijima, S. Helical microtubules of graphitic carbon. *Nature* **1991**, *354*, 56–58. [[CrossRef](#)]
2. Popov, V.N. Carbon nanotubes: Properties and application. *Mater. Sci. Eng. R* **2004**, *43*, 61–102. [[CrossRef](#)]
3. Tjong, S.C. Recent progress in the development and properties of novel metal matrix nanocomposites reinforced with carbon nanotubes and graphene nanosheets. *Mater. Sci. Eng. R* **2013**, *74*, 281–350. [[CrossRef](#)]
4. Esawi, A.M.; Farag, M.M. Carbon nanotube reinforced composites: Potential and current challenges. *Mater. Des.* **2007**, *28*, 2394–2401. [[CrossRef](#)]

5. Chen, B.; Li, S.; Imai, H.; Jia, L.; Umeda, J.; Takahashi, M.; Kondoh, K. Load transfer strengthening in carbon nanotubes reinforced metal matrix composites via in situ tensile tests. *Compos. Sci. Technol.* **2015**, *113*, 1–8. [[CrossRef](#)]
6. Chen, B.; Li, S.; Imai, H.; Jia, L.; Umeda, J.; Takahashi, M.; Kondoh, K. Carbon nanotube induced microstructural characteristics in powder metallurgy Al matrix composites and their effects on mechanical and conductive properties. *J. Alloy. Compd.* **2015**, *651*, 608–615. [[CrossRef](#)]
7. He, C.; Zhao, N.; Shi, C.; Du, X.; Li, J.; Li, H.; Cui, Q. An Approach to Obtaining Homogeneously Dispersed Carbon Nanotubes in Al Powders for Preparing Reinforced Al-Matrix Composites. *Adv. Mater.* **2007**, *19*, 1128–1132. [[CrossRef](#)]
8. Jiang, L.; Fan, G.; Li, Z.; Kai, X.; Zhang, D.; Chen, Z.; Humphries, S.; Heness, G.; Yeung, W.Y. An approach to the uniform dispersion of a high volume fraction of carbon nanotubes in aluminum powder. *Carbon* **2011**, *49*, 1965–1971. [[CrossRef](#)]
9. Liu, Z.Y.; Xiao, B.L.; Wang, W.G.; Ma, Z.Y. Singly dispersed carbon nanotube/aluminum composites fabricated by powder metallurgy combined with friction stir processing. *Carbon* **2012**, *50*, 1843–1852. [[CrossRef](#)]
10. Chen, B.; Li, S.; Imai, H.; Jia, L.; Umeda, J.; Takahashi, M.; Kondoh, K. An approach for homogeneous carbon nanotube dispersion in Al matrix composites. *Mater. Des.* **2015**, *72*, 1–8. [[CrossRef](#)]
11. Uozumi, H.; Kobayashi, K.; Nakanishi, K.; Matsunaga, T.; Shinozaki, K.; Sakamoto, H.; Tsukada, T.; Masuda, C.; Yoshida, M. Fabrication process of carbon nanotube/light metal matrix composites by squeeze casting. *Mater. Sci. Eng. A* **2008**, *495*, 282–287. [[CrossRef](#)]
12. Shin, S.E.; Bae, D.H. Strengthening behavior of chopped multi-walled carbon nanotube reinforced aluminum matrix composites. *Mater. Charact.* **2013**, *83*, 170–177. [[CrossRef](#)]
13. Esawi, A.M.K.; Morsi, K.; Sayed, A.; Gawad, A.A.; Borah, P. Fabrication and properties of dispersed carbon nanotube-aluminum composites. *Mater. Sci. Eng. A* **2009**, *508*, 167–173. [[CrossRef](#)]
14. Poirier, D.; Gauvin, R.; Drew, R.A.L. Structural characterization of a mechanically milled carbon nanotube/aluminum mixture. *Compos. Part A Appl. Sci. Manuf.* **2009**, *40*, 1482–1489. [[CrossRef](#)]
15. Stein, J.; Lenczowski, B.; Anglaret, E.; Fréty, N. Influence of the concentration and nature of carbon nanotubes on the mechanical properties of AA5083 aluminium alloy matrix composites. *Carbon* **2014**, *77*, 44–52. [[CrossRef](#)]
16. Saheb, N.; Iqbal, Z.; Khalil, A.; Hakeem, A.S.; Aqeeli, N.A.; Laoui, T.; Al-Qutub, A.; Kirchner, R. Spark plasma sintering of metals and metal matrix nanocomposites: A review. *J. Nanomater.* **2012**, *2012*, 18. [[CrossRef](#)]
17. Chen, B.; Jia, L.; Li, S.; Imai, H.; Takahashi, M.; Kondoh, K. In Situ Synthesized Al4C3 Nanorods with Excellent Strengthening Effect in Aluminum Matrix Composites. *Adv. Eng. Mater.* **2014**, *16*, 972–975. [[CrossRef](#)]
18. Zhan, G.-D.; Kuntz, J.; Wan, J.; Garay, J.; Mukherjee, A.K. Alumina-based nanocomposites consolidated by spark plasma sintering. *Scr. Mater.* **2002**, *47*, 737–741. [[CrossRef](#)]
19. Kwon, H.; Estili, M.; Takagi, K.; Miyazaki, T.; Kawasaki, A. Combination of hot extrusion and spark plasma sintering for producing carbon nanotube reinforced aluminum matrix composites. *Carbon* **2009**, *47*, 570–577. [[CrossRef](#)]
20. Chen, B.; Kondoh, K.; Imai, H.; Umeda, J.; Takahashi, M. Simultaneously enhancing strength and ductility of carbon nanotube/aluminum composites by improving bonding conditions. *Scr. Mater.* **2016**, *113*, 158–162. [[CrossRef](#)]
21. Kondoh, K.; Fukuda, H.; Umeda, J.; Imai, H.; Fugetsu, B. Microstructural and mechanical behavior of multi-walled carbon nanotubes reinforced Al-Mg-Si alloy composites in aging treatment. *Carbon* **2014**, *72*, 15–21. [[CrossRef](#)]
22. Aquilanti, V.; Mundim, K.C.; Elango, M.; Kleijn, S.; Kasai, T. Temperature dependence of chemical and biophysical rate processes: Phenomenological approach to deviations from Arrhenius law. *Chem. Phys. Lett.* **2010**, *498*, 209–213. [[CrossRef](#)]

